



AMERICAN METEOROLOGICAL SOCIETY

[HOME](#) [SEARCH](#) [HELP](#) [FEEDBACK](#) [SUBSCRIBE](#) [CURRENT ISSUES](#) [ARCHIVE](#) [AMS WEBSITE](#)

[\[Print Version\]](#) [\[Create Reference\]](#) [\[Search AMS Glossary\]](#)

TABLE OF CONTENTS

[\[1. Introduction\]](#) [\[2. Methods\]](#) [\[3. Results\]](#) [\[4. Discussion\]](#) [\[5. Summary and...\]](#) [\[References\]](#) [\[Tables\]](#) [\[Figures\]](#)

doi: 10.1175/1520-0426(2004)021<1044:ASMODT>2.0.CO;2

Journal of Atmospheric and Oceanic Technology: Vol. 21, No. 7, pp. 1044–1058.

A Simple Method of Deriving Three-Dimensional Temperature Fields Using Remotely Sensed and In Situ Data for Application to Numerical Hydrodynamic Models of Estuaries and Bays

Timothy R. Keen and Richard W. Gould

Oceanography Division, Naval Research Laboratory, Stennis Space Center, Mississippi

Jean-Francois Cayula and Walton E. McBride

Planning Systems Inc., Stennis Space Center, Mississippi

John P. Blaha

Naval Oceanographic Office, Stennis Space Center, Mississippi

Clark Rowley

Oceanography Division, Naval Research Laboratory, Stennis Space Center, Mississippi

(Manuscript received 6 November 2002, in final form 23 October 2003)

ABSTRACT

This paper describes the subjective interpolation method (SIM) for generating three-dimensional temperature distributions from remotely sensed sea surface temperature (SST) fields. SIM incorporates MATLAB-based cloud removal software and a method of generating synthetic temperature profiles based on observations. This approach depends on the human facility for recognizing patterns in complex images. Three-dimensional temperature fields produced by SIM are compared to analogous fields based on optimal interpolation (OI) methods by using temperature fields interpolated by the two methods to initialize a baroclinic coastal ocean circulation model. The initial SST surface fields from both methods have a bias of less than -0.5°C and rms errors of less than 1.5°C . After running for 48 h, the bias and rms errors for the OI simulations are 0.3° and 1.2°C , respectively, whereas the same errors for the SIM run are 0.7° and 0.9°C . The OI and SIM approaches can be combined to allow preprocessing of SST data in three steps: 1) bad pixels can be marked by a human user (quality control), 2) automated OI methods can be used to produce valid SST fields based on available reference data, and 3) the SST field can be projected into the water column using a combination of observed and synthetic profiles.

1. Introduction [Return to TOC](#)

Remotely sensed ocean variables have proven useful in evaluating both physical and biological processes in the coastal ocean, especially when used in conjunction with in situ measurements (e.g., [Arnone and Gould 2001](#) ; [Walker and Hammack 2000](#) ; [Schofield et al. 2002](#) ; [Glenn and Grassle 2000](#)). The combined use of these data has also improved the predictions of numerical ocean circulation models (e.g., [Ezer and Mellor 1997](#)). One of the most significant applications of remote sensing to numerical models has been the assimilation of sea surface temperature (SST). Despite the improvements associated with incorporating these data in open-ocean models, there is still much work to be done to improve numerical simulations of the coastal ocean.

a. Background

The operational satellite sensor systems produce data of varying resolution and quality. The polar orbiting Advanced Very High Resolution Radiometer (AVHRR) satellites have a pixel size of order 1 km and provide SST precision of order 0.15°C . Present Geostationary Operational Environmental Satellites (GOES) and GOES variable (GVAR) infrared systems are able to deliver 4-km pixels. GOES SST data are generally less accurate than AVHRR, with an SST precision of order 0.2°C . Whereas a two-satellite AVHRR system potentially yields four looks at the same region during a 24-h period, a single *GOES-8* system yields potentially 48 looks at the same region. Multiple ocean color observing satellite systems also exhibit differing characteristics in temporal and spatial resolution.

Multichannel AVHRR data are combined to form the Multi-Channel Sea Surface Temperature (MCSST) database ([Barton et al. 1989](#)). A nonlinear SST algorithm (NLSST) that incorporates an initial estimate of the SST field is in common use today. The Naval Oceanographic Office generates MCSST (NLSST) products using multiple pixels, which are combined to form averages with spatial resolutions that vary from 50 km for global fields to 4 km for local products. MCSST products from other organizations have similar resolutions. This procedure produces a more uniform product but removes the kilometer-scale variability observed in the original data. This averaging is not a serious problem for larger areas, but it can obscure important processes such as river plumes in coastal areas ([Walker et al. 1996](#)). Previous studies have led to several conclusions with respect to using AVHRR-derived SST: 1) the SST measurement is of the skin temperature and not the bulk temperature ([Schluessel et al. 1990](#)); 2) atmospheric water vapor partly affects the retrieval of SST, but no independent water vapor datasets are used in the algorithm ([Emery et al. 1994](#)); and 3) cloud masking can be minimized by taking the warmest pixel at a fixed location over all images within 1 week. The logic is that clouds are “cold,” and they move much farther in 1 week than ocean features. This last point has led to the use of compositing in producing SST retrievals for operational use.

Operational ocean prediction systems use remotely sensed SST and satellite altimetry in numerical models to varying degrees ([Anderson and Robinson 2000](#); [Rhodes et al. 2002](#); [Gangopadhyay and Robinson 2002](#)). However, extending SST data downward within the water column using only a few measurements remains problematical. In the deep ocean, the availability of

databases and the dominance of geostrophic flow allow the use of statistical approaches ([Carnes et al. 1990](#) ; [Mitchell et al. 1996](#)). The generation of temperature profiles is further aided by the moderately slow changes in ocean temperature away from the coast. Thus, assimilation of satellite sea surface height and sea surface temperature is routinely used today with good results for deep-basin mesoscale circulation modeling ([Fox et al. 2002](#) ; [Rhodes et al. 2002](#)).


The U.S. Navy coastal ocean forecasting program aims to maximize the use of remotely sensed and in situ data for ocean circulation, surface wave, and turbidity modeling. In support of this objective, several methods of combining model predictions and observations have been developed under the Northern Gulf of Mexico Littoral Initiative (NGLI), which is implementing an ocean forecasting system using high-resolution numerical models ([Ahsan et al. 2002a ,b](#) ; [Blumberg et al. 2000](#)). NGLI uses airborne and satellite remotely sensed data for SST, salinity, and turbidity for ocean model evaluation and model initialization and assimilation ([Blaha et al. 2000](#) ; [Gould et al. 2001 , 2002](#)). Although comprehensive measurement programs have been conducted on the U.S. continental shelf [e.g., the Louisiana–Texas Shelf Physical Oceanography Program (LATEX)], most coastal data are not generally available for use in developing statistical methods such as optimal interpolation (OI) utilizing satellite-derived SST. This is especially true for areas outside the continental United States.

Previous work indicates the usefulness of developing methods for deriving three-dimensional temperature and salinity fields in the coastal ocean ([Keen and Murphy 1999](#) ; [Keen and Walker 1998](#) ; [Keen and Arnone 1997](#)), but these methods are dependent on the availability of remotely sensed ocean surface variables. The current study explores techniques used to employ remote sensing data from AVHRR, GOES, the Sea-viewing Wide Field-of-view Sensor (SeaWiFS), and airborne sensors for initializing shallow-water circulation models. Sampling difficulties are a major impediment to coastal ocean data assimilation. Temporal and spatial variability of water properties on the inner shelf and within estuaries arises from wind setup, river discharge, and inshore intrusions of offshore waters. This variability demands high-resolution observations. However, those satellite systems able to spatially resolve this variability of sea surface temperature and ocean color suffer from the blocking effects of clouds.

Adding to the difficulty of acquiring cloud-free remotely sensed fields of SST in coastal areas is the problem that sea surface sensing systems do not reveal the vertical stratification of the water column. For example, stratification of temperature and salinity increases during periods of low winds and away from channels (where tidal flow is stronger). Wintertime mixing effects remove vertical stratification in shallow estuaries while increasing horizontal stratification across the shelf. One reason for using high-resolution surface observations (1-km AVHRR-derived SST) for model initialization is that archived in situ observations show vertical gradients that correlate to surface observations in some domains. In these cases, ascribing the vertical gradient information to the observed surface data enables three-dimensional fields of temperature and salinity to be generated for initial conditions. It is likely that studies of this correlation will permit the derivation of a more accurate, physically realistic stratification in coastal waters.

b. Objective

The preceding paragraphs indicate the immensity of the problem of assimilating remotely sensed and in situ data into numerical coastal ocean circulation models. In light of these difficulties, this paper will address a small but important part of the problem. Before any attempt can be made to produce realistic three-dimensional temperature distributions, it is necessary to have a complete description of the surface temperature field. Therefore, the primary objective of this paper is to describe a straightforward method of building a three-dimensional temperature field that may be used to evaluate and initialize high-resolution baroclinic numerical models of estuaries and coastal seas. In order to effectively utilize this method, a simple technique for projecting this surface distribution downward into the water column is described.

The method will be demonstrated using AVHRR-derived SST fields from the Mississippi bight region ([Fig. 1](#) ). In an attempt to evaluate the utility of this technique, it will be compared to a statistical approach (OI) using model simulations initialized using both OI and the method described herein. Temperature fields are the initial focus but the method is equally applicable to salinity, suspended solids, and water optical clarity as well.

2. Methods [Return to TOC](#)

The method of producing realistic three-dimensional fields of temperature described in this paper entails two steps: 1) correcting available SST fields from AVHRR for missing data due to clouds and 2) extrapolating the two-dimensional SST fields into the subsurface using either measured or synthetic temperature profiles. The method described herein is applicable to any surface field. However, it has been developed to address specific problems that have occurred in our efforts to initialize coastal circulation models.

This method is applied to 1-km AVHRR-derived SST fields only. This high-resolution product is necessary in order to capture the potential SST variability within the study area. Furthermore, only individual SST products are considered, even though composites may be necessary at some locations and times. This study thus focuses on the most difficult assimilation problem. A fundamental assumption of this approach is that it is necessary to capture the observed variability in SST. This assumption is probably not justified for simulating large regions; however, the Mississippi bight study area encompasses only 2° of longitude. Furthermore, within this domain, the exchange of cold water through narrow channels between barrier islands separating the open water of the bight and the enclosed water of Mississippi Sound is important. This focus dictates the use of the highest-resolution SST fields that can be acquired.


In order to evaluate the usefulness of the declouding software described in this paper, it is compared to a more traditional method. Optimal interpolation is typically used for large areas where climatologies exist (e.g., [Fox et al. 2002](#)). It will be used in this study to produce cloud-free SST fields using the same data as are available to the manual declouding program user. The interpolated temperature fields will be assimilated into a coastal circulation model, which will permit a realistic assessment of the utility of the OI and decloud methods.

a. A Matlab-based graphical user interface for image editing

The manual processing technique described in this section is intended to allow the user (e.g., coastal modeler) to replace missing and bad values in high-resolution remotely sensed data based on a subjective analysis of the recent history of SST in the area as well as fronts, eddies, and filaments that may be visible in the data. Thus, this technique is hereinafter called the subjective interpolation method (SIM). The results of applying SIM are not

repeatable, even by the same user, as are those from a statistical approach like OI. Nevertheless, it is considered a reasonable alternative to not utilizing the available imagery and, thus, being forced to use inaccurate data from another time period or, worse, a single profile for the entire region. There is no mathematical rationale for the method described herein, but it does utilize available data to approximate the missing values. Furthermore, because the missing values are selected based on the user's evaluation of the available data, they are not randomly determined from a mathematical algorithm that has no functional relationship to the data.


This section discusses algorithms that have been developed to simplify the manual editing procedure. The user does not need to be a skilled remote sensing analyst because a checklist acts as a guide to decision making during the editing process. However, the more knowledgeable user will undoubtedly produce a better SST field. The editing guidelines, which are based on principles of image analysis, compose as small a number of steps as possible.

The graphical user interface (GUI) and cloud-editing algorithms have been developed using MATLAB. The main menu includes a menu window (not shown), which provides menus to adjust declouding parameters, derive subsurface layers, navigate the image, and print. The GUI also includes a main image window (Fig. 2 ) , which displays the field that will be declouded with a color bar. The buttons on the left allow for various manipulations; zooming, adding temperature contours, deforming, the field and filling a region are the most frequently used operations. The user may also find it useful to overlay a coastline and temperature contours. Typically, the user compares the SST field to be declouded with SST fields from previous days, or from other sources such as GOES, microwave imagery, and climatology. If a reference image is available, it is also useful to display the temperature contours of the reference image on the main image or display the reference image itself.

Problems in SST images fall into three main categories: 1) cloud cover, 2) sensor corruption near land, and 3) errors in navigation of the remote sensing image before processing it for SST. Clouds can occur either in open water or partly over land. Corruption near land can often be corrected using offshore SST values. Navigation errors require considerable care to correct and may necessitate reprocessing of the original image if they are large.

The image declouding software uses three primary modes of operation: contour deformation, filling, and eddy placement. These features are described in this section. In addition to the description in the text, these modes are controlled by user-set parameters. Parameters for the deformation, fill, and eddy modes are adjusted in the “parameter” pulldown menu from the menu window.

1) CONTOUR DEFORMATION

Contour deformation is useful in bringing offshore water to the coast to avoid problems of temperature corruption near the coast. Contour deformation mode is selected by clicking the left mouse button (MB1) on the “deform” button on the main menu (Fig. 2 ). The process of contour deformation is relatively simple; the user selects the origin and destination points by clicking MB1 on the selected points within the image. It is important to note that during this process, neighbors of the origin and destination points are affected to various degrees by the deformation process. All points that fall within a selected distance of the origin point are affected: features in front of the origin point with respect to the deformation are compressed while features behind are expanded.

Mathematically, the contour deformation process can be defined as follows. Defining \mathbf{x}_1 and \mathbf{x}_2 as the coordinates of the origin and destination points, respectively, gives \mathbf{V} , the displacement vector given by

$$\mathbf{V} = \mathbf{x}_2 - \mathbf{x}_1. \quad (1)$$

The adjusted length nv is given by

$$nv = |\mathbf{V}| E, \quad (2)$$

where E is an influence constant that is set to 1.5 by default. If it is assumed that \mathbf{x}_{p1} are the initial coordinates of a neighboring point, the distance between the neighboring point and the origin point is

$$d = |\mathbf{x}_{p1} - \mathbf{x}_1|. \quad (3)$$

After deformation of the field, the neighboring point is moved to its final

coordinates:

$$\mathbf{x}_{p2} = \mathbf{x}_{p1} + \left(1 - \frac{d}{nv}\right)\mathbf{V}, \quad \text{for } 1 - \frac{d}{nv} > 0. \quad (4)$$

The last step of the contour deformation process is to interpolate the deformed field to a uniformly spaced grid. As an example of contour deformation, the coastal clouds seen in [Fig. 3a](#) are removed by bringing offshore water over land. Note, however, that the eddy south of the coast should not be deformed; thus, the contour deformation process is completed in a series of small displacements that avoid affecting the neighboring eddy. The resultant SST field ([Fig. 3b](#)) contains a few artifacts, which can be removed ([Fig. 3c](#)) using filling as discussed in the next section.

2) FILLING



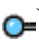
The fill operation consists of delineating a region with multiple clicks of button MB1, and doing a cubic interpolation (the default) of the region based on Delaunay triangulation ([Yang 1986](#), 446–449). The set of points to be interpolated consists of all \mathbf{x} such that

$$\begin{aligned} v(\mathbf{x}) &< \max[v(\mathbf{x}_c)] + T \quad \text{and} \\ v(\mathbf{x}) &> \min[v(\mathbf{x}_c)] - T, \end{aligned} \quad (5)$$


where $v(\mathbf{x}_c)$ is the value at each selected point \mathbf{x}_c , $v(\mathbf{x})$ is the value at location \mathbf{x} , and T is a tolerance. The selected points \mathbf{x}_c are joined to form Delaunay triangles, which are used in interpolating to the new points \mathbf{x} . [Equation \(5\)](#) guarantees that $v(\mathbf{x})$ falls between the minimum and maximum selected values within a prescribed tolerance. The use of a tolerance T permits the interpolated value to vary slightly from the values at the triangle vertices and permits a smoother transition between the actual and interpolated fields. The tolerance T is found from

$$T = \{\max[v(\mathbf{x}_c)] - \min[v(\mathbf{x}_c)]\} \cdot (0.01). \quad (6)$$


The fill mode is entered by clicking the “fill” button on the main menu ([Fig. 2](#)) with button MB1. Vertices for the region to be contoured are selected by

clicking button MB1 at all selected points (Fig. 4a ). Clicking the middle mouse button (MB2) closes the contour and starts the filling process. Clicking the right mouse button (MB3) cancels the fill process. The fill procedure can produce artifacts (Fig. 4b ), which can be removed by smoothing (Fig. 4c ). When dealing with a large cloud-covered region, it may be difficult to find good vertices, in which case it is possible to bring cloud-free values into the cloud-covered region with contour deformation. For large cloud-covered regions, it is important to look at images from previous days or other sensors to estimate the underlying structure.

3) ADDING EDDIES

The third mode that can be used to complete missing structures in the input field is entered by clicking button MB1 on the “eddy” button on the main menu (Fig. 2 ). This mode can be used to add a circular feature of a prescribed size and magnitude anywhere on the image. This mode should be used to correct images where there is clear evidence of the existence of an eddy that is mostly obscured by cloud cover. After adding an eddy, it should be modified to blend with the background field using the fill and contour deformation modes.

b. Generating temperature profiles

The primary application of this software is to generate accurate three-dimensional temperature fields for assimilation into high-resolution numerical models. This means that a subsurface temperature distribution must also be generated. To assist in generating complete three-dimensional fields, a simple algorithm has been added to the decloud software to project the SST into the water column. Temperature profiles in coastal areas are highly variable, as seen in typical profiles from the Mississippi bight measured during an NGLI cruise in January 2000 (Fig. 5 ). The profiles with colder water at the surface were measured within the sound and reflect inflow from rivers. Ongoing work is examining methods of incorporating profile data when generating three-dimensional temperature distributions (e.g., [Gangopadhyay et al. 2003](#)), but this effort is beyond the scope of the present study. [Keen and Murphy \(1999\)](#) discuss some methods of accomplishing this if sufficient profile data are available. For now, the user has the option of controlling the specific structure of the regional profile with user-set parameters in a parametric profile model.

The subsurface layers are generated from an exponential equation:

$$T(z) = \frac{T_s - T_B}{1 + A \exp(z - z_{ML})} + T_B, \quad (7)$$

where T_s and T_B are the surface and bottom temperatures, respectively; z_{ML} is the depth of the mixed layer; and A is an exponential coefficient that is used to adjust the shape of the depth profile. The parameters T_B , A , and Z_{ML} are adjusted by selecting “parameters for 3D temperatures” from the “3D” pulldown menu on the menu window. By default, the depth of the mixed layer Z_{ML} is set to 4 m, the bottom temperature T_B is set to 16.52°C, and the exponential coefficient A is set to 0.85. The surface temperature T_s is taken from the corrected SST field. These parameters may be modified to better match observed conditions. Subsurface layers are output at predetermined depth levels z set by the user in a file named `dform_3d.m`. [Equation \(7\)](#) can produce a large range of temperature profiles ([Fig. 6](#)) that are similar to those from the Mississippi bight. It is thus a reasonable representation of the temperature profiles found in the coastal ocean. It is up to the user to determine the optimal profiles for their application.

c. Optimal interpolation

Traditionally, oceanographers have resorted to climatologies derived from available historical data to generate three-dimensional fields of temperature (e.g., [Teague et al. 1990](#)). Recently developed statistical tools like the Modular Ocean Data Assimilation System (MODAS; [Fox et al. 2002](#)) supplement these climatologies by merging data from disparate sources such as satellites, historical ship measurements, and profiles. The method presently employed by MODAS to combine these data is OI ([Bretherton et al. 1976](#)), which is a common technique for combining an initial background field and measured data using a model of how nearby data are correlated. The correlation is often assumed to have a simple exponential or Gaussian form that includes length and time scales. Given an initial estimate of the field and its error, a set of data points with estimated errors, and climatology of the area, the OI technique provides a set of weights to apply to the data. The result is a new estimate of the field, including an estimate of its accuracy.

The MODAS system contains two quality control routines for observations: 1) a cross-validation method based on an assumed error correlation model and 2) a method that normalizes the observation's deviation from a background field using the known climate variability and estimated background error.

[Method 2](#)) rejects observations with normalized deviations that are larger than a prescribed value. In the analysis performed for this study, observations with deviations larger than 2.5 times the climate variability or background error are not used in the analysis.


d. Model simulation approach



The applicability of interpolated SST fields to numerical modeling is examined using numerical simulations of coastal flow and temperature in the Mississippi bight that use SST fields to derive three-dimensional temperature initial conditions. The interval of interest in this study is 0000 UTC 15 January–0000 UTC 19 January. The purpose of the numerical simulations is to evaluate the effect of using interpolated temperature fields in this shallow water region. This objective is complicated, however, because cloud-free AVHRR images with temporal spacing of order 48 h were not available for this study. Thus it is necessary to synthesize SST fields using a numerical model. This is considered to be a reasonable approach because the purpose of this study is to evaluate the OI and SIM techniques and not the numerical model, which is treated as ground truth for this purpose.

The OI and SIM techniques are compared in the following manner. First, a baseline model simulation is run with a three-dimensional temperature initial condition generated from a relatively cloud-free image and the synthetic temperature profiles discussed above. This model runs for the entire 96-h period and SST fields are saved at 48 and 96 h. An artificial cloud is added to the 48-h SST field (0000 UTC 17 January) using the eddy feature of the declouding program ([Fig. 7](#)). This idealized cloud has a temperature that is 10°C lower than the original data. The halo around the cloud is similar to the halos observed in AVHRR images that are affected by clouds. The OI method is applied to this SST field using the 0000 UTC 15 January SST field as the background, and climatological variability as the assumed background error variance. This interpolation is performed on the surface distribution only because the purpose is to compare the two methods of correcting cloud errors. Therefore, profiles are calculated using [Eq. \(7\)](#). The SIM is also performed on the SST field from the model at 0000 UTC 17 January. The numerical model

is then run in parallel simulations for 17–19 January with the temperature distributions from the OI and SIM techniques. The initial and final SST fields from these parallel simulations are discussed below.

The output from the declouding program consists of hierarchical data format (HDF) or text files. These files are checked for completeness before passing them to the numerical model. It is also a prerequisite that the input temperature fields are spatially larger than the model grid. This is important because the satellite images are processed by other agencies, which are unaware of later applications of the data; thus, the regional coverage of the AVHRR fields may vary significantly between consecutive images. Merging several fields to cover larger areas, or preprocessing the images before declouding, may be required.


The Princeton Ocean Model (POM; [Oey and Chen 1992](#)) is used in this study. The POM solves the primitive equations for momentum, as well as salinity, temperature, turbulent energy, and a turbulence length scale ([Mellor and Yamada 1982](#)). This model uses split modes; a small time step is used to solve for the depth-integrated flow (external or barotropic mode) and a larger time step is used to compute three-dimensional variables (internal or baroclinic mode). The model uses a terrain-following σ -coordinate system in the vertical. The input to POM can include bathymetry, initial three-dimensional salinity and temperature fields, heat and momentum fluxes at the surface, and the water surface anomalies, transports, and temperature and salinity values at open boundaries. The simulations are run on a Cartesian grid with cell sizes of 777 and 898 m along the x and y axes, respectively ([Fig. 1](#) ). There are 11 sigma levels in the vertical and the maximum water depth is 280 m, which only occurs at the southeastern corner of the grid. Most water depths within the Mississippi bight are less than 50 m.

Atmospheric forcing for this study consists of wind stresses only. Uniform winds measured at National Oceanographic and Atmospheric Administration (NOAA) buoy 42007 ([Fig. 8](#) ; see [Fig. 1](#)  for location) are used for the model simulations described below. No heat fluxes are applied to the POM because of the uncertainty of these calculations in coastal areas, especially for short simulations. This simplification is considered reasonable because of the focus of this work on the interpolation techniques rather than the numerical model. The Naval Oceanographic Office compiled the bottom topography from a variety of sources, including the National Ocean Service 3" database.

The POM has an open boundary condition that includes the following: 1) tidal elevations and depth-integrated transports from the Advanced Circulation (ADCIRC) database for the East Coast and Gulf of Mexico ([Leutlich et al. 1992](#)), 2) relaxation of temperature to the initial condition on inflow, and 3) a radiation condition for both baroclinic and barotropic waves generated within the model domain ([Flather 1976](#)). No river inflow is used for these simulations and the salinity is constant at 35 psu.

3. Results [Return to TOC](#)

The time period used for the model simulations was selected based on the availability of relatively cloud-free AVHRR images with sufficient thermal structure to examine the influence of the OI and SIM interpolation approaches on model-predicted SST. The atmospheric forcing from 15 to 19 January 2002 is also important in evaluating the relative impacts of model-induced mixing and transport on the predicted temperature distributions.

The simulation interval is characterized by weak and variable winds during the prefrontal phase of a front that passed over the region during 18–19 January, with peak winds at buoy 42007 of 10.6 m s^{-1} at 0400 UTC 19 January ([Fig. 8](#) ). The wind rotated clockwise at about one revolution per day prior to frontal passage. The baseline model simulation begins on 15 January, when the winds were from the southwest at 3.1 m s^{-1} . The wind speed remained weak until 0000 UTC 17 January, at which time the SST field from the model was used to generate new three-dimensional temperature fields. Finally, the wind steadily increased on 18 January and reached a speed of 9.3 m s^{-1} with a northwesterly bearing as the front passed. The wind speed weakened during the postfrontal phase and reached a minimum of less than 1 m s^{-1} on 21 January.

a. Flow and SST predicted by the baseline simulation

This discussion of coastal flow within the Mississippi bight is intended to demonstrate the effect of local advection and vertical mixing on the simulated SST distribution. Thus, the focus is on the simulated currents and water levels on 17 January rather than on examining the detailed flow during the entire 4-

day period of the baseline simulation. This will allow the important hydrodynamic forcing to be elucidated. The POM applied to this region has been validated in a previous study using tidal and wind-driven currents and water levels ([Keen 2002](#)).

The simulated flow within this region ([Fig. 9](#)) is dominated by a diurnal tide with a range of less than 1 m. The tidal wave propagates from east to west, entering Mississippi Sound near Mobile Bay and exiting through Chandeleur Sound in the southwest. Maximum currents of more than 0.5 m s^{-1} are predicted within the passes between barrier islands. Overall, because of the weak winds on 17 January, surface currents in the open water of the bight are primarily tidal with predicted magnitudes of less than 0.3 m s^{-1} . Despite the weak flow, the Mellor–Yamada turbulence closure in POM predicts moderate vertical mixing, which acts to weaken the thermocline and deteriorate the SST prediction for runs longer than 24 h if surface heat flux and open-ocean boundary conditions are not applied.

The impact of vertical mixing in the POM can be seen in maps of the evolving SST field from the model ([Fig. 10](#)). The SST field at 0000 UTC 15 January ([Fig. 10a](#)) reveals a curved filament of 17°C water within the bight. There is also some intrusion into the eastern end of Mississippi Sound because of tidal mixing at the passes between barrier islands. The surface temperature inside the enclosed western waters is approximately 10°C . This SST field is not used in the interpolation simulations, but it is used as climatology for applying the OI method. It is also used as a reference image for the SIM technique.

The temperature of the filament has decreased to less than 13°C on 17 January ([Fig. 10b](#)) because of turbulent mixing and advection in POM. However, the fundamental structure of the feature persists. The temperature inside the eastern Mississippi Sound has increased slightly with the introduction of warmer water by tidal intrusion. There is also evidence that warmer water has passed over the shoal at the southern end of the Chandeleur Islands. This SST field will be used to derive the initial conditions for the interpolation runs that are discussed below.

The SST field on 19 January ([Fig. 10c](#)) retains the basic outline of the warm filament. Furthermore, the mean temperature of the feature remains

above 12°C, although its edges are less distinct. A few patches of slightly elevated temperatures (less than 1°C above background) are also predicted at the landward coast within western Mississippi Sound. This is remnant offshore water moving with the mean tidal flow. A warmer filament (about 1.5°C elevated) is also propagating up the sound side of the Chandeleur Islands. By the end of the 4-day simulation, the influence of the original warm offshore filament can be seen throughout the sounds, but it has not penetrated into the extreme western reaches of Mississippi Sound.

The changes in SST predicted by the baseline simulation are due to horizontal advection by surface flow (Fig. 9) and by vertical turbulent mixing by current shear. This process is represented by the Mellor–Yamada mixing model, which has been shown to reasonably reproduce mixing in stratified water (e.g., Burchard et al. 1998; Keen and Glenn 1998). The large temperature gradient introduced into the numerical model by the 17°C surface water of the filament is not matched by a salinity gradient in the model. Thus, turbulent mixing dramatically reduces the SST field within 48 h (Fig. 11). This surface cooling is accompanied by deepening of the thermocline, but the weak surface flow during the simulation period does not erode stratification further. The persistence of stratification indicates that the results are meaningful. It is expected that a time-dependent open boundary condition and including salinity profile data would significantly improve the model predictions.

b. SST predicted by the optimal interpolation simulation

The POM as used in these simulations is run in prognostic mode, which means that all of the variables are computed, whereas temperature and salinity are typically held fixed for the diagnostic mode. Thus, the computed baroclinic currents for the OI and SIM simulations are significantly different from the baseline simulation, which started 2 days earlier with a different temperature field. Nevertheless, the magnitudes of the simulated currents in the OI and SIM simulations will be similar to those presented in Fig. 9 because of the dominance of tidal and wind-driven flow in the simulations. This section, as well as the next section on the SIM simulation, will, therefore, focus on the predicted SST distributions only. The currents predicted by the OI and SIM simulations are very similar and will not be discussed. Although hydrodynamic adjustment to the temperature artifacts introduced by interpolation methods can be important, it is beyond the scope of the present

study because baroclinic flow is weak in these simulations. This question is more important for studies of strongly baroclinic flows such as coastal jets.

The SST field generated by the OI method for 17 January ([Fig. 12a](#)) shows some significant differences from the baseline model. The warm filament that is seen in the baseline run ([Fig. 10b](#)) has been cut off, producing an eddy with a higher temperature than in the baseline SST field. This interpolated field has a bias of approximately -0.4°C (the OI temperature is lower than the baseline) and an rms error of 1.52°C (see [Table 1](#)). This partly reflects the choice of weighting factors used in the interpolation as well as the method used to determine which cells have valid SST values. This problem is examined in more depth in [section 4](#).

The impact of higher SSTs on subsurface temperature is evident in the profile on 17 January ([Fig. 13a](#)), which shows a 3.5°C SST anomaly at the center of the cloud. An additional error has been introduced in the subsurface temperatures of the OI and SIM simulations by using [Eq. \(7\)](#) to calculate profiles instead of using the profiles from the baseline run. This error is an artifact of the experimental design, which uses a numerical model to supply baseline SST fields rather than a remotely sensed estimate. This study is not examining subsurface error, however, and the same technique was used for both the OI and SIM temperature profiles. Thus, the additional error in simulated SST fields due to stratification will not introduce a bias for either interpolation method. Nevertheless, it is useful to be aware that there will be some influence of this subsurface error for these experiments.

The numerical model acts to smooth out perturbations in the SST field through vertical mixing and advection. Thus, the SST field predicted by the OI simulation on 19 January ([Fig. 12b](#)) has a lower bias (less negative) and a smaller rms error ([Table 1](#)) than on 17 January. The warm eddy remains, however, because of the weak horizontal mixing and the temperature stratification ([Fig. 13b](#)), which damps the vertical turbulent mixing. Most of the error is due to this persistent eddy, which is apparent in the 1.2°C anomaly at the surface on 19 January. Stratification is persistent in the OI simulation and SST remains 1°C higher than in the baseline run. Note that SST has increased by about 0.5°C in the baseline run, rather than decreasing, because of the shoreward advection of warmer water. This advection is masked in the OI run by vertical mixing with water from a depth of 5 m, which is below the thermocline.

c. SST predicted by the subjective interpolation method simulation

The SIM technique, as applied using the declouding software, permits the user to select which points are valid using subjective criteria. Thus, using the same reference image as the OI method (Fig. 10a), the user determines that the warm filament should be continuous rather than being cut off to form an eddy as in Fig. 12a. The resulting SST field (Fig. 14a) on 17 January more closely resembles the baseline run (Fig. 10b). This similarity is reflected in an SST bias of less than -0.3°C and an rms error of less than 1°C (Table 1). The relatively small error is caused by the lower temperature values that have been interpolated into the artificial cloud area. The SIM approach always uses fill values that are proximal to the bad pixel, which prevents large values from being calculated based on climatology or distant cells within the image. The temperature profile on 17 January (Fig. 13a) reveals an error of less than 1°C at the surface whereas the subsurface profile reflects the use of Eq. (7) rather than the profile from the baseline run.

The warm filament is barely discernable in the SST field from the SIM simulation on 19 January (Fig. 14b) and the temperature is cooler as well. The generally lower temperature relative to the baseline run is visible in the profile (Fig. 13b). This lower SST is caused by mixing with water from below the thermocline as in the OI run. The resultant SST bias, however, has increased to -0.71°C , which is higher than the bias of the OI run. The rms error has also increased but not by as much. The larger SST bias and rms error is caused by vertical mixing with water from beneath the thermocline.





4. Discussion [Return to TOC](#)

The problem of preprocessing AVHRR images to remove the effects of clouds, land, and navigation errors can be decomposed into two fundamental steps: 1) identify bad pixels (quality control) and 2) interpolate from regions of good pixels to replace the bad values. The OI and SIM approaches are quite similar in how they address step 2 in this study, because of the availability of a good image from only 48 h prior to the analysis. This similarity of interpolation methods is why the SST fields seen in Figs. 12a and 14a resemble each other except for the dissection of the warm filament by the OI technique (Fig. 12a).

The primary difference between these methods is in the selection of the values to use in the interpolation; the OI method uses the field from the reference image in a statistical manner whereas the user makes this selection in SIM. In order for bad pixels to be identified by the automated cross-validation method, they must have unique values. This does not occur in the artificial cloud in [Fig. 7](#). The nearly uniform values within the cloud are well correlated and thus pass the cross-validation test. The second quality control method rejects observations with normalized deviations that are larger than a prescribed value. Values inside the cloud are properly rejected by this method, but cold temperatures in the cloud halo are passed to the OI analysis. In addition, the general surface temperature cooling between the 15 January field, which is used as background for the OI analysis, and the 17 January field that was used as data ([Fig. 10](#)), caused the quality control to reject some of the valid pixels. The apparent SST change over 48 h is not unusual for the shallow-water coastal domain simulated in this experiment. More sophisticated and conservative algorithms for removing cloud contamination are used in operational processing of AVHRR SST data, but they produce datasets with lower horizontal resolution that do not preserve small-scale features. The SIM user, however, has no difficulty identifying the SST pattern associated with the cloud and thus removes all of the questionable pixels.

The SIM technique allows the user to determine which pixels are valid (quality control) and modify them based on available imagery and personal experience. Because of this subjectivity, however, there are significant issues regarding the robustness of the interpolated fields. This study does not examine these questions, which can only be properly addressed by perceptual tests like those conducted as part of software applications development (e.g., [Wegenkittl et al. 1997](#); [Trafton et al. 2000](#); [Vickery 2003](#)). However, this subjectivity is also the strength of the SIM approach because of the facility with which human beings can derive information from complex images. In this respect, the greatest advantage of SIM is the ability of the user to recognize bad pixels.

The SST fields predicted by the OI and SIM simulations differ from the baseline because of the initial errors introduced by preprocessing, and the nonlinear interaction of the interpolated three-dimensional temperature fields with the circulation. The feedback between the temperature field and the flow can be treated as vertical and horizontal processes. Horizontal feedback is not

as important in this study because the flow field is dominated by tidal and wind-forced circulation. The effect of vertical feedback is seen in the different response of the interpolated runs compared to the baseline. The baseline profile on 17 January (line in [Fig. 13a](#) ) reflects a longer history of mixing whereas the OI (solid square in [Fig. 13a](#) ) and SIM (solid circle in [Fig. 13a](#) ) runs have temperature profiles that are not in equilibrium with the turbulence and flow fields. Thus, by 19 January the temperature field in the baseline run (line in [Fig. 13b](#) ) contains warmer water near the surface because of advection within the mixed layer whereas the interpolated runs have not yet developed equilibrium temperature profiles.

The Mississippi bight encompasses shallow bays, estuaries, and open-shelf environments. The temperature field varies both spatially and temporally between and within these local environments. This study focuses on a warm filament in the open-shelf environment because of the availability of good AVHRR images with visible features. The presence of rivers, barrier islands, shallow sounds, and deepwater eddies and filaments is common in coastal areas; therefore, the Mississippi bight is a representative coastal area with respect to the temperature field. The ability of the SIM approach to perform slightly better than the OI method indicates that this is a useful technique for initializing temperature distributions. It is expected that its skill over other methods will improve in more complex coastal environments or in cases where data are sparser, because of the ability of humans to identify the important patterns in the remotely sensed images.

In determining the usefulness of the SIM technique, one must first determine the importance of accurately assimilating SST into numerical models. The coastal temperature field is important for understanding biological processes like the development of harmful algal blooms, primary production associated with thermal fronts, and the health of shellfish beds. Thus, it is necessary to accurately predict the temperature field even when it does not dominate the coastal flow. However, in the case of strong baroclinic flows as in estuaries and coastal jets, there are direct effects that occur on subkilometer scales. Being able to assimilate SST or surface salinity into models of this phenomenon would clearly improve the accuracy of simulations of these processes (e.g., [Xu et al. 2002](#)).

5. Summary and conclusions [Return to TOC](#)

This paper describes a method for removing cloud artifacts from AVHRR-derived SST fields. The cloud-editing software is based on MATLAB products and thus offers graphical user interfaces that allow interactive and intuitive manipulation of the satellite-derived fields. This work also describes a method of generating synthetic temperature profiles based on observations in nearshore water. The subjective interpolation method (SIM) is based on human skill at recognizing patterns in complex images whereas automated methods like optimal interpolation (OI) rely on climatology and available data to complete both quality control and interpolation functions.

The usefulness of the three-dimensional temperature fields produced by SIM is demonstrated by comparison between matched simulations with the Princeton Ocean Model. A baseline simulation was completed for 15–19 January 2002 using an SST image from 15 January to produce an initial condition. The model-predicted SST on 17 January was then used to produce new SST fields after a large cloud was inserted. This “clouded” SST field was then processed using OI and SIM techniques and matched simulations are completed for 17–19 January. The initial SST fields produced by both methods contain considerable variability that cannot be captured by simpler methods of deriving initial conditions. Both initial SST surface fields have a bias of less than -0.5°C and rms errors of less than 1.5°C . After running for 48 h, the bias and rms errors for the OI simulation are 0.3° and 1.2°C , respectively, whereas the same errors for the SIM run are 0.7° and 0.9°C .

This method will prove most useful for coastal areas where the highest-resolution SST data are required. The SIM approach is a general method that should be equally applicable for other ocean variables such as salinity and suspended solids. It is not generally applicable to large regions, however, where MCSST-based OI methods do not have the same problems of quality control that occur in this study. The best approach is to take advantage of the human facility for pattern recognition in completing the quality control step and use automated OI methods to produce valid fields. Furthermore, it is important to incorporate observations wherever possible in generating temperature profiles.

Acknowledgments. This work was funded by the Northern Gulf of Mexico Littoral Initiative of the Naval Oceanographic Office. The first author was also supported by Program Element 0601153N sponsored by the Office of Naval Research. Clark Rowley was supported by the Oceanographer of the

Navy via the Space and Naval Warfare Systems Command (PMW155).

REFERENCES [Return to TOC](#)

- Ahsan, Q., and Coauthors, 2002a: Northern Gulf of Mexico Littoral Initiative modeling program. *Proc. Seventh Int. Conf. on Estuarine and Coastal Modeling*, St. Petersburg, FL, ASCE, 949–965.
- Ahsan, Q., A. F. Blumberg, L. Honghai, W. W. Schroeder, and C. Szczechowski, 2002b: Forecasting the environment of the littoral waters in the northern Gulf of Mexico. *Proc. Seventh Int. Conf. on Estuarine and Coastal Modeling*, St. Petersburg, FL, ASCE, 966–981.
- Anderson, L. A., and A. R. Robinson, 2000: Physical and biological modeling in the Gulf Stream region: I. Data assimilation methodology. *Deep-Sea Res.*, **47A**, 1787–1827. [Links ▶](#)
- Arnone, R. A., and R. W. Gould, 2001: Mapping coastal processes with optical signatures. *Backscatter.*, **12**, 17–24.
- Barton, I. J., A. M. Zavody, D. M. O'Brien, D. R. Cutten, R. W. Saunders, and D. T. Lewellynjones, 1989: Theoretical algorithms for satellite-derived sea-surface temperatures. *J. Geophys. Res.*, **94**, D33365–3375. [Links ▶](#)
- Blahe, J. P., and Coauthors, 2000: Gulf of Mexico ocean monitoring system. *Oceanography.*, **13**, 210–17. [Links ▶](#)
- Blumberg, A. F., Q. Ahsan, and J. K. Lewis, 2000: Modeling the hydrodynamics of the Mississippi Sound and adjoining rivers, bays and shelf waters. *Proc. Oceans 2000 Conf.*, Marine Technology Society, 177–189.
- Bretherton, F. P., R. E. Davis, and C. B. Fandry, 1976: A technique for objective analysis and design of oceanographic experiments applied to MODE-73. *Deep-Sea Res.*, **23**, 559–582. [Links ▶](#)
- Burchard, H., O. Peterson, and T. P. Rippeth, 1998: Comparing the performance of the Mellor–Yamada and the $k-\epsilon$ turbulence models. *J.*

Geophys. Res., **103**, C510543–10554. [Links ▶](#)

Carnes, M. R., J. L. Mitchell, and P. W. DeWitt, 1990: Synthetic temperature profiles derived from Geosat altimetry: Comparison with air-dropped expendable bathythermograph profiles. *J. Geophys. Res.*, **95**, 17979–17992. [Links ▶](#)

Emery, W., Y. Yu, and G. Wick, 1994: Correcting infrared satellite estimates of sea surface temperature for atmospheric water vapor attenuation. *J. Geophys. Res.*, **99**, C35219–5236. [Links ▶](#)

Ezer, T., and G. L. Mellor, 1997: Data assimilation experiments in the Gulf Stream region: How useful are satellite-derived surface data for nowcasting the subsurface fields. *J. Atmos. Oceanic Technol.*, **14**, 1379–1391. [Links ▶](#)

Flather, R. A., 1976: A tidal model of the north-west European continental shelf. *Mem. Roy. Sci. Soc. Liège.*, **10**, 141–164.

Fox, D. N., C. N. Barron, M. R. Carnes, M. Booda, G. Peggion, and J. V. Gurley, 2002: The Modular Ocean Data Assimilation System (MODAS). *Oceanography.*, **15**, 22–28. [Links ▶](#)

Gangopadhyay, A., and A. R. Robinson, 2002: Feature-oriented regional modeling of oceanic fronts. *Dyn. Atmos. Oceans.*, **36**, 201–232. [Links ▶](#)

Gangopadhyay, A., A. R. Robinson, P. J. Haley, W. G. Leslie, C. J. Lozano, J. J. Bisagni, and Z. Yu, 2003: Feature-oriented regional modeling and simulations in the Gulf of Maine and Georges Bank. *Cont. Shelf Res.*, **23**, 317–353. [Links ▶](#)

Glenn, S. M., and J. F. Grassle, 2000: A well-sampled ocean. *Oceanus.*, **42**, 28–30. [Links ▶](#)

Gould, R. W. Jr., T. R. Keen, R. A. Arnone, R. H. Stavn, and A.-R. Diercks, 2001: Bio-optical variability in a barrier-island coastal environment: Coupling remote sensing imagery, shipboard measurements, and modeling results. *Extended Abstracts, Ocean Odyssey 2001*, Mar del Plata, Argentina, IAPSO–IABO, IB05-40. [Available online at www.iugg.org/iapso/abstracts/IB-

[05/IB05-40.htm.](#)]

Gould, R. W. Jr., R. A. Arnone, S. D. Ladner, P. M. Martinolich, A.-R. Diercks, and R. H. Stavn, 2002: Optical variability linked to physical forcing in the northern Gulf of Mexico using satellite, shipboard, and CODAR observations. *Eos, Trans. Amer. Geophys. Union*, **83** (Suppl.), Abstract OS12J-06.

Keen, T. R., 2002: Waves and currents during a winter cold front in the Mississippi bight, Gulf of Mexico: Implications for barrier island erosion. *J. Coastal Res.*, **18**, 622–636. [Links ▶](#)

Keen, T. R., and R. A. Arnone, 1997: Assimilating 1 km AVHRR data into a relocatable coastal ocean forecast model. *Eos, Trans. Amer. Geophys. Union.*, **78**, (Suppl.), F354 [Links ▶](#)

Keen, T. R., and S. M. Glenn, 1998: Factors influencing model skill for hindcasting shallow water currents during Hurricane Andrew. *J. Atmos. Oceanic Technol.*, **15**, 221–236. [Links ▶](#)

Keen, T. R., and N. D. Walker, 1998: Modeling a coastal squirt in the Gulf of Mexico. *Eos, Trans. Amer. Geophys. Union.*, **79**, (Suppl.), F408 [Links ▶](#)

Keen, T. R., and S. Murphy, 1999: Developing a relocatable coastal ocean forecast model. *Proc. Oceanology Int. 99 Pacific Rim*, Singapore, Spearhead Exhibitions, 47–58.

Leutlich, R. A., J. J. Westerink, and N. W. Schreffner, 1992: ADCIRC: An advanced three-dimensional circulation model for shelves, coasts, and estuaries. Report 1: Theory and methodology of ADCIRC-2DDI and ADCIRC-3DI. Tech. Rep. DRP-92-6, Department of the Army, 168 pp.

Mellor, G. L., and T. Yamada, 1982: Development of a turbulence closure model for geophysical fluid problems. *Rev. Geophys.*, **20**, 851–875. [Links ▶](#)

Mitchell, H. L., C. Chouinard, C. Charette, R. Hogue, and S. J. Lambert, 1996: Impact of a revised analysis algorithm on an operational data assimilation system. *Mon. Wea. Rev.*, **124**, 1243–1255. [Links ▶](#)

Oey, L., and P. Chen, 1992: A nested-grid ocean model: With application to the simulation of meanders and eddies in the Norwegian coastal current. *J. Geophys. Res.*, **97**, 20063–20086. [Links ▶](#)

Rhodes, R. C., and Coauthors, 2002: Navy real-time global modeling systems. *Oceanography.*, **15**, 29–43. [Links ▶](#)

Schluessel, P., W. J. Emery, H. Grassl, and T. Mammen, 1990: On the skin-bulk temperature difference and its impact on satellite remote sensing of sea surface temperature. *J. Geophys. Res.*, **95**, 13341–13356. [Links ▶](#)

Schofield, O., T. Bergmann, P. Bissett, J. F. Grassle, D. B. Haidvogel, J. Kohut, M. Moline, and S. M. Glenn, 2002: The long-term ecosystem observatory: An integrated coastal observatory. *IEEE J. Oceanic Eng.*, **27**, 146–154. [Links ▶](#)

Teague, W. J., M. J. Carron, and P. J. Hogan, 1990: A comparison between the generalized digital environmental-model and Levitus climatologies. *J. Geophys. Res.*, **95**, C57167–7183. [Links ▶](#)

Trafton, J. G., S. S. Kirschenbaum, T. L. Tsui, R. T. Miyamoto, J. A. Ballas, and P. D. Raymond, 2000: Turning pictures into numbers: Extracting and generating information from complex visualizations. *Int. J. Human–Comput. Stud.*, **53**, 827–850. [Links ▶](#)

Vickery, R. J., 2003: New visualization techniques for multi-dimensional variables in complex physical domains. Ph.D. thesis, Mississippi State University, Starkville, MS, 116 pp.

Walker, N. D., and A. B. Hammack, 2000: Impacts of winter storms on circulation and sediment transport: Atchafalaya–Vermillion Bay region, Louisiana, U.S.A. *J. Coastal Res.*, **16**, 996–1010. [Links ▶](#)

Walker, N. D., O. K. Huh, L. J. Rouse, and S. P. Murray, 1996: Evolution and structure of a coastal squirt off the Mississippi River delta: Northern Gulf of Mexico. *J. Geophys. Res.*, **101**, C920643–20655. [Links ▶](#)

Wegenkittl, R., H. Löffelmann, and E. Gröller, 1997: Visualizing the behavior of higher dimensional dynamical systems. *Proc. Visualization '97*, Phoenix, AZ, ACM, 119–125.

Xu, J., S. Y. Chao, R. R. Hood, R. Raleigh, H. V. Wang, and W. C. Boicourt, 2002: Assimilating high-resolution salinity data into a model of a partially mixed estuary. *J. Geophys. Res.*, **107**, 3074, doi:10.1029/2000JC000626.

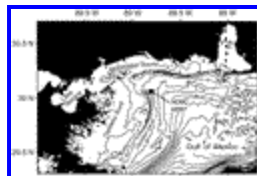
Yang, T. Y., 1986: *Finite Element Structural Analysis*. Prentice-Hall International Series in Civil Engineering and Engineering Mechanics, Prentice Hall, 464 pp.

Tables [Return to TOC](#)

TABLE 1. SST error (°C) for OI and SIM simulations.

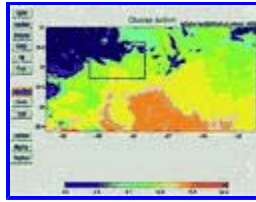
	OI		SIM	
	17 Jan	19 Jan	17 Jan	19 Jan
Mean error	0.3695	0.2750	0.2854	0.7136
Rms error	1.5180	1.198	0.9077	0.9220

Figures [Return to TOC](#)



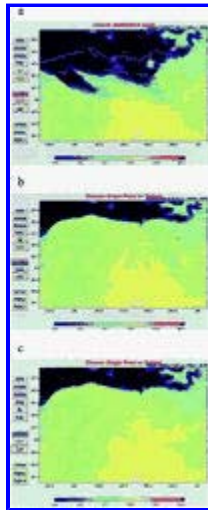
[Click on thumbnail for full-sized image.](#)

FIG. 1. Map of the Mississippi bight region; the numerical model grid covered the entire area.



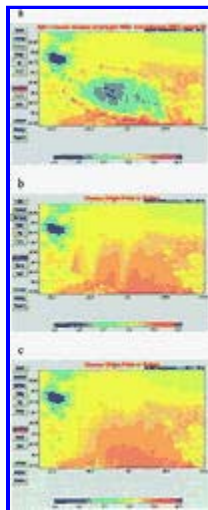
Click on thumbnail for full-sized image.

FIG. 2. MATLAB GUI with example of unprocessed image. The box indicates the inset shown in [Fig. 3](#). Clouds and land are indicated by black.



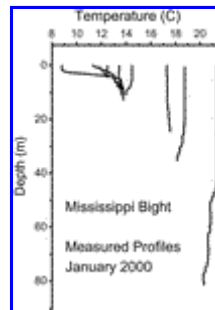
Click on thumbnail for full-sized image.

FIG. 3. (a) Start of contour deformation process; origin point is shown at 30°N, 89°W. (b) After a few moves, the offshore water is brought inland. (c). Artifacts left after the contour deformation process have been removed with region filling. Clouds and land are indicated by black.



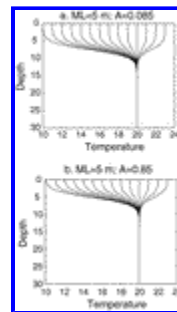
[Click on thumbnail for full-sized image.](#)

FIG. 4. (a) Selecting vertices for a fill operation to remove a small cloud. (b) Artifacts can be minimized by choosing vertices more carefully or by applying region filling to a subarea of the field. (c) Declouded area with artifacts smoothed out.



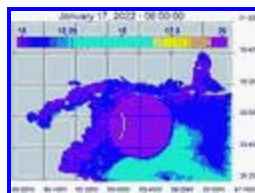
[Click on thumbnail for full-sized image.](#)

FIG. 5. Typical temperature profiles measured within the Mississippi bight during Jan 2000.



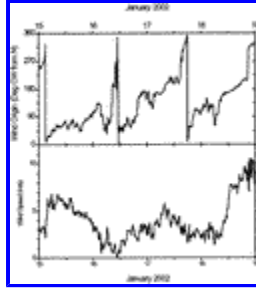
[Click on thumbnail for full-sized image.](#)

FIG. 6. Synthetic temperature profiles calculated from Eq. (7) for two values of the parameter A ; ML = mixed layer depth.



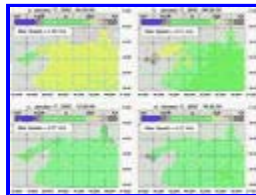
[Click on thumbnail for full-sized image.](#)

FIG. 7. SST map from 17 Jan with an artificial cloud (violet circle) centered at 29.7°N , 88.4°W .



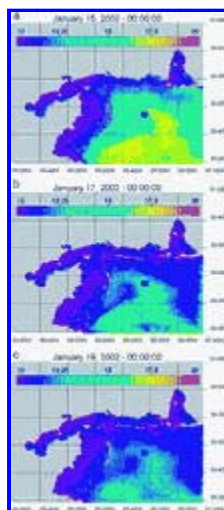
[Click on thumbnail for full-sized image.](#)

FIG. 8. Wind direction and speed measured at NOAA buoy 42007 in the Mississippi bight.




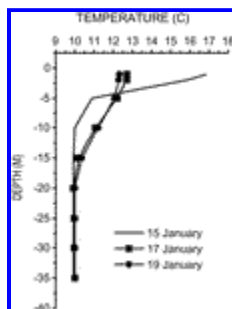
[Click on thumbnail for full-sized image.](#)

FIG. 9. Snapshots of surface currents (vectors) overlaid on the sea surface height anomaly (contoured) predicted by the baseline simulation at 6-h intervals on 17 Jan 2002. The color bar is for the sea surface anomaly (m).



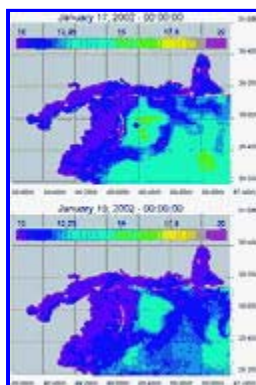
[Click on thumbnail for full-sized image.](#)

FIG. 10. SST ($^{\circ}\text{C}$) maps from the baseline model: (a) 0000 UTC 15 Jan, (b) 0000 UTC 17 Jan, and (c) 0000 UTC 19 Jan. The solid square indicates the location of the temperature profiles in [Fig. 11](#) .



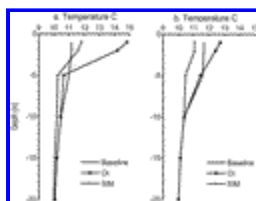
Click on thumbnail for full-sized image.

FIG. 11. Profiles of temperature from the baseline model at 0000 UTC on 15, 17, and 19 Jan. See [Fig. 10](#) for location.



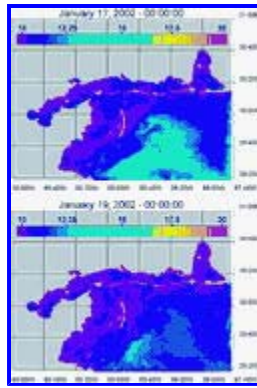
Click on thumbnail for full-sized image.

FIG. 12. Maps of SST ($^{\circ}\text{C}$) predicted by the OI simulation: (a) 0000 UTC 17 Jan and (b) 0000 UTC 19 Jan. The solid circle indicates the location of the profiles in [Fig. 13](#).



Click on thumbnail for full-sized image.

FIG. 13. Temperature profiles predicted by the baseline (line only), OI (solid square), and SIM (solid diamond) simulations: (a) 0000 UTC 17 Jan and (b) 0000 UTC 19 Jan. See [Fig. 12](#) for location of the profiles.



Click on thumbnail for full-sized image.

FIG. 14. Maps of SST ($^{\circ}\text{C}$) predicted by the SIM simulation: (a) 0000 UTC 17 Jan and (b) 0000 UTC 19 Jan.

Corresponding author address: Dr. Timothy R. Keen, Naval Research Laboratory, Code 7322, Stennis Space Center, MS 39529. E-mail: keen@nrlssc.navy.mil

© Copyright by American Meteorological Society 2004